Manuscript prepared for Atmos. Chem. Phys. Discuss.
with version 2014/09/16 7.15 Copernicus papers of the LaTeX class copernicus.cls.
Date: 16 February 2016

Evaluation of the ACCESS-Chemistry Climate Model for the Southern Hemisphere

K. A. Stone[1,2], O. Morgenstern[3], D. J. Karoly[1,2], A. R. Klekociuk[4,5], W. J. R. French[4,5], N. L. Abraham[6,7], and R. Schofield[1,2]

[1]School of Earth Sciences, University of Melbourne, Melbourne, Australia
[2]ARC Centre of Excellence for Climate System Science, Sydney, Australia
[3]National Institute of Water and Atmospheric Research, Lauder, New Zealand
[4]Australian Antarctic Division, Hobart, Australia
[5]Antarctic Climate and EcoSystems Cooperative Research Centre, Hobart, Australia
[6]National Centre for Atmospheric Science, UK
[7]Centre for Atmospheric Science, Department of Chemistry, University of Cambridge, Cambridge, CB2 1EW, UK

Correspondence to: K. A. Stone (stonek@student.unimelb.edu.au)

Abstract

Chemistry climate models are important tools for addressing interactions of composition and climate in the Earth System. In particular, they are used for assessing the combined roles of greenhouse gases and ozone in Southern Hemisphere climate and weather. Here we present an evaluation of the Australian Community Climate and Earth System Simulator-Chemistry Climate Model, focusing on the Southern Hemisphere and the Australian region. This model is used for the Australian contribution to the international Chemistry-Climate Model Initiative, which is soliciting hindcast, future projection and sensitivity simulations. The model simulates global total column ozone (TCO) distributions accurately, with a slight delay in the onset and recovery of springtime Antarctic ozone depletion, and consistently higher ozone values. However, October averaged Antarctic TCO from 1960 to 2010 show a similar amount of depletion compared to observations. Comparison with model precursors shows large improvements in the representation of the Southern Hemisphere stratosphere, especially in TCO concentrations. A significant innovation is the evaluation of simulated vertical profiles of ozone and temperature with ozonesonde data from Australia, New Zealand and Antarctica from 38 to 90° S. Excess ozone concentrations (greater than 26 % at Davis and the South Pole during winter) and stratospheric cold biases (up to 10 K at the South Pole during summer and autumn) outside the period of perturbed springtime ozone depletion are seen during all seasons compared to ozonesondes. A disparity in the vertical location of ozone depletion is seen: centered around 100 hPa in ozonesonde data compared to above 50 hPa in the model. Analysis of vertical chlorine monoxide profiles indicates that colder Antarctic stratospheric temperatures (possibly due to reduced mid-latitude heat flux) are artificially enhancing polar stratospheric cloud formation at high altitudes. The model's inability to explicitly simulate supercooled ternary solution may also explain the lack of depletion at lower altitudes. Analysis of the simulated Southern Annular Mode (SAM) index compares well with ERA-Interim data, an important metric for correct representation of Australian climate. Accompanying these modulations of the SAM, 50 hPa zonal wind differences between 2001–2010 and 1979–1998 show increasing zonal wind strength south-

ward of 60° S during December for both the model simulations and ERA-Interim data. These model diagnostics shows that the model reasonably captures the stratospheric ozone driven chemistry-climate interactions important for Australian climate and weather while highlighting areas for future model development.

1 Introduction

Coupled chemistry-climate models are designed to address the interactions between atmospheric chemistry and the other components of the climate system. This involves the interactions between ozone, greenhouse gases (GHGs), and the dynamics of climate and weather. Improved understanding of these links is important for the Australian region due to the regular springtime Antarctic ozone depletion and its role in modulating Southern Hemisphere surface climate. The Australian region will be affected by these interactions over the course of this century due to ozone recovery as well as changes in GHGs (e.g Thompson et al. (2011); Arblaster and Gillett. (2014). Thus, global collaborations, such as the currently ongoing Chemistry-Climate Model Initiative (CCMI) (Eyring et al., 2013b) and past chemistry climate modelling projects, which focus on process-oriented evaluation of model performance, will help shape our understanding of future Australian weather and climate.

The annual springtime depletion of Antarctic ozone is attributed to the anthropogenic emissions of ozone-depleting substances (ODSs), mostly chlorofluorocarbons (CFCs), the presence of the polar vortex, and the formation of polar stratospheric clouds (PSCs) within it (Solomon, 1999). In 1987, the Montreal Protocol was signed to phase out the production and release of ODSs into the atmosphere. This has been very effective in halting and reversing the build-up of halogens in the stratosphere, with ozone depletion presently not strengthening anymore, and peaking around the year 2000 (Dameris et al., 2014). Other recent studies have noted a detection in ozone recovery (e.g. Shepherd (2014); de Laat (2015). Antarctic ozone depletion over the previous half century has had a significant influence, equal to GHG increases, on Southern Hemisphere tropospheric climate during summer, mostly through the cooling of the stratosphere by ozone depletion affecting the

Southern Annular Mode (SAM) in the late spring and summer, thus shifting surface wind patterns (Gillett and Thompson, 2003; Shindell and Schmidt, 2004; Arblaster and Meehl, 2006; Thompson et al., 2011; Canziani et al., 2014). Another obvious surface impact, important for ecosystems, is an increase in ultra violet (UV) radiation reaching the surface (WMO, 2011, 2014). Therefore, future climate change in the Australian region is expected to be influenced both by stratospheric ozone recovery and by changes in GHG concentrations (Arblaster et al., 2011). Anthropogenic emissions of GHGs are also expected to influence stratospheric ozone concentrations, both through their dynamical and their chemical effects. GHG-induced cooling of the stratosphere is expected to contribute to an increase in the rate of ozone recovery by slowing gas-phase ozone loss reactions (Barnett et al., 1975; Jonsson et al., 2004). A warming troposphere and associated changes in wave activity propagation from the troposphere into the stratosphere are also predicted to speed up the Brewer–Dobson circulation (Butchart et al., 2006). Thus, the combined effects of a cooler stratosphere and a strengthening of the Brewer–Dobson circulation, causing a speedup of tropical stratospheric ozone advection to mid-latitudes, is expected to reduce the recovery rate in tropical stratospheric ozone, or even cause tropical ozone to decrease again later this century (Austin et al., 2010), and produce a larger recovery trend in the mid-latitudes (Shepherd, 2008; Li et al., 2009).

A simulation of these interacting processes is required to fully capture and assess the impact of future ozone recovery alongside increasing GHGs for many aspects of Australian climate, such as westerly winds and Southern Australian rainfall patterns. The Australian Community Climate and Earth-System Simulator-Chemistry Climate Model (ACCESS-CCM) is used to produce hindcast and future projections, as well as sensitivity simulations to help address these questions and contribute to the CCMI project. CCMI is designed to bring together the current generation of global chemistry models. This includes chemistry-transport and chemistry-climate models (CCMs), some of which are coupled to an interactive ocean, to perform simulations to an agreed standard to help address questions relating to chemistry-climate interactions and inform future ozone assessments and Intergovernmental Panel on Climate Change (IPCC) reports. It also follows on from past

chemistry climate modelling comparisons, such as the Chemistry Climate Model Validation (CCMVal) activity (SPARC-CCMVal, 2010), the Atmospheric Chemistry and Climate Model Inter-comparison Project (ACCMIP) (Lamarque et al., 2013), and Atmospheric Chemistry and Climate Hindcast (AC&C Hindcast) simulations which informed the 5th Assessment Report of IPCC.

In this paper we describe the key components of the model we have used in our contribution to CCMI, which marks the first Australian contribution to an international chemistry-climate modelling project. Advancements from the direct ACCESS-CCM precursors, The Unified Model/United Kingdom Chemistry and Aerosols Module-University of Cambridge (UMUKCA-UCAM) and The Unified Model/United Kingdom Chemistry and Aerosols Module-Met Office (UMUKCA-METO) are discussed. We also describe the two main simulation setups used in this paper for the evaluation of the model. These include hindcast historical simulations and future projections. An evaluation of the model performance and an analysis of the simulation output, focusing on the Southern Hemisphere, are described. Emphasis is placed on diagnosing the model performance through analysis of ozone and temperature vertical profiles at Australian, New Zealand and Antarctic sites. Analysis of diagnostics related to climate impacts most relevant to the Australian region, such as shifting surface winds through analysis of the SAM metric and the stratospheric polar vortex are also included.

2 Model description

The model is based on New Zealand's National Institute of Water and Atmospheric Research (NIWA) version of the United Kingdom Chemistry and Aerosols (UKCA) chemistry-climate model (NIWA-UKCA) (Morgenstern et al., 2009, 2014). It includes the HadGEM3 background climate model in the Global Atmosphere (GA) 2 configuration (Hewitt et al., 2011), with the UKCA module for the chemistry component (Morgenstern et al., 2013; O'Connor et al., 2014). It also incorporates the United Kingdom Meteorological Office's (UKMO) Surface Exchange Scheme-II (MOSES-II). The model setup does not currently

incorporate an interactive coupled ocean model; instead, prescribed time-evolving sea surface temperatures (SSTs) and sea ice concentrations (SICs) are used. The model is run at an N48 (3.75° longitude by 2.5° latitude) horizontal resolution and L60 (60 hybrid height levels) vertical resolution with a model top of 84 km.

HadGEM3 has a non-hydrostatic setup (Davies et al., 2005) and a semi-Lagrangian advection scheme (Priestley, 1993). Gravity wave drag is made up of both an orographic gravity wave drag component (Webster et al., 2003) and a parameterised spectral gravity wave drag component, representing the non-orographic components (Scaife et al., 2002). Radiation is described by Edwards and Slingo (1996) and has nine bands in the long-wave part of the spectrum ranging from 3.3 µm to 1.0 cm and six bands in the short-wave part of the spectrum ranging from 200 nm to 10 µm.

The UKCA module includes both stratospheric and tropospheric chemistry with 90 chemical species, including species involved in O_x, NO_x, HO_x, BrO_x, and ClO_x chemical family chemistry (Banerjee et al., 2014; Archibald et al., 2011). Appropriate species undergo dry and wet deposition. The chemical species undergo over 300 reactions, including bimolecular, termolecular, photolysis, and heterogeneous reactions on polar stratospheric clouds (PSCs). The model assumes two different kinds of PSCs, namely type II water ice and type Ia nitric acid trihydrate (NAT); which is assumed to be in equilibrium with gas phase nitric acid (HNO_3). Both undergo irreversible sedimentation, causing dehydration and denitrification of the polar vortex during winter (Morgenstern et al., 2009). Type 1b supercooled ternary solution of H_2SO_4-H_2O-HNO_3 (STS) PSCs are not explicitly simulated. However, reactions on the surface of liquid sulpuric acid are included. Photolysis reactions are calculated by the FASTJX scheme (Neu et al., 2007; Telford et al., 2013).

The ACCESS-CCM model is a direct successor to the UMUKCA-UCAM and UMUKCA-METO CCMs that contributed to CCMVal-2, the second iteration of CCMVal. A number of advancements to the model where made since. Regarding the stratospheric chemistry scheme, the UMUKCA models and ACCESS-CCM both follow Morgenstern et al. (2009), with only minor adjustments made to include the halogenated very short lived substances: CH_2Br_2 and $ChBr_3$, and update the advection of total nitrogen. Other more major changes

to the chemistry in ACCESS-CCM are the introduction of FASTJX instead of FAST-J2 (Bian and Prather, 2002), the introduction of tropospheric chemistry, approximately doubling the number of species and reactions from those in the stratospheric scheme (O'Connor et al., 2014), and the addition of isoprene for tropospheric chemistry. In addition, the UMUKCA models used HadGEM1 as the background climate model, with the major updates in HadGEM3 being to the convection, cloud and boundary layer schemes, among others, described in Hewitt et al. (2011).

The model runs evaluated in this paper include the CCMI hindcast run, labeled REF-C1 from 1960–2010 and the historical part of a future projection run, labeled REF-C2 from 1960–2010 (Eyring et al., 2013b). For the REF-C1 run, SSTs and SICs are gridded fields based on observations from the Hadley Centre HaDISST dataset (Rayner et al., 2003). GHGs are from Meinshausen et al. (2011) and Riahi et al. (2011) and follow the Representative Concentration Pathway 8.5 (RCP 8.5) after 2005. RCP 8.5 represents a greenhouse gas concentration pathway that will result in a mean predicted radiative forcing of 8.5 $\mathrm{W\,m^{-2}}$ at the top of the atmosphere by 2100 relative to pre-industrial values. RCP 8.5 was chosen as this scenario best represents the observations between 2005–2010. ODSs follow the emission scenario that is balanced across all sources (A1B scenario) from WMO (2011). Anthropogenic and biofuel emissions follow Granier et al. (2011). Biomass burning emissions follow van der Werf et al. (2006); Schultz et al. (2008) and Lamarque et al. (2011). For the REF-C2 run, the only change before 2000 is that SSTs and SICs are climate model estimates taken from a HadGEM2-ES r1p1i1 CMIP5 model run (Jones et al., 2011). After 2000, all forcings follow RCP 6.0, as this was the beginning of a harmonisation period for emissions (2000–2005) (Meinshausen et al., 2011). RCP 6.0 was chosen following the CCMI REF-C2 specifications (Eyring et al., 2013b).

3 Observational and model datasets

Evaluation of the model is undertaken by comparing output to different observation and model datasets, described below.

3.1 Total column ozone database

Simulated total column ozone (TCO) is evaluated against the monthly averaged Bodeker Scientific TCO database (Bodeker et al., 2005; Müller et al., 2008). This database is assimilated from satellite observations and spans the period from 1979–2012, where dataset offsets and drifts have been accounted for using Dobson and Brewer ground-based observations. This has the advantage of including the stable and long-term Dobson and Brewer measurements. However, it is important to note that the version of the dataset used includes interpolation. Therefore, a limitation of this comparison is the shortage of wintertime observations. This is because of the satellite-assimilated data only being available in sunlit hours, which is in clear deficiency during the Antarctic winter.

3.2 CCMVal-2

The CCMVal-2 project is described extensively in SPARC-CCMVal (2010), and was designed as a coordinated inter-comparison of eighteen chemistry climate models that performed hindcast historical, future projection, and sensitivity simulations. This project included precursors to the ACCESS-CCM model, such as the UMUKCA-UCAM and UMUKCA-METO models, with the model improvements since then described in Sect. 2. CCMI serves as the next iteration of the CCMVal project, with improved chemistry climate models. We use the historical simulations from the CCMVal-2 dataset, from 1960 to 2005, labeled REF-B1, as well as UMUKCA-UCAM and UMUKCA-METO CCMVal-2 simulations, to compare time-series of Antarctic TCO, stratospheric temperature, and stratospheric winds from the REF-C1 and the historical part of the REF-C2 simulation.

3.3 CMIP5

The Coupled Model Inter-comparison Project Phase 5 (CMIP5) evaluates coupled ocean-atmosphere models (Taylor et al., 2012), and includes some chemistry climate models. We use the recent past (1960–2005) of the historical simulations from CMIP5 models that used

prescribed ozone in the comparison of the seasonal SAM index for the REF-C1 and the historical period of the REF-C2 simulations.

3.4 ERA-Interim

ERA-Interim re-analysis data, from the European Centre for Medium-Range Weather Forecasts (ECMWF), is used to compare stratospheric temperature and wind time series from the recent past with the REF-C1 and the recent past segment of the REF-C2 simulations. Observations in conjunction with a forecast model are used to create the dataset (Dee et al., 2011), which spans the period of 1979 to present.

3.5 Ozonesondes

Ozonesondes are balloon-borne instruments that measure the vertical structure of ozone, along with other parameters such as temperature, pressure and humidity over an observation site, typically up to an altitude of around 35 km. In this study we have used electrochemical cell (ECC) ozonesondes at five locations, namely: Melbourne (37.5° S, 145° E), Lauder, NZ (45° S, 169.7° E), Macquarie Island (54.6° S, 158.9° E), Davis (68.5° S, 79° E) and South Pole (90° S, 169° E). Typically, ozonesonde accuracy has been stated to be at 5% (SPARC, 1998), but generally ranges between 5–10% for ECC ozonesondes when following a standardised procedure (Smit et al. 2007).

3.6 Microwave Limb Sounder

The Microwave Limb Sounder (MLS) instrument onboard the Aura satellite is used to evaluate vertical profiles of chlorine monoxide (ClO) over the Antarctic region (Santee et al., 2008; Livesey et al., 2011). The Aura satellite orbits in a sun-synchronous orbit with an inclination of 98.2°. The MLS ClO measurements are scientifically useful within the vertical range of 147–1 hPa and comparison of the model data with the MLS ClO measurements has taken into account all data quality control considerations, such as, precision, quality, status flag and convergence (see Livesey et al. (2011)). The data covers the period from late

2004–present. Comparison with the model data has also taken into account the MLS ClO a priori profiles and retrieved averaging kernels to ensure that the two datasets are sampled consistently, this is done following Eq. 1.2 in Livesey et al. (2011)), where the model data is modified to represent what MLS would observe. This is done by taking the difference between the model and a priori profiles, multiplying them with the averaging kernels, and adding the product to the a priori.

4 Model evaluation

To evaluate the performance of the model in the Southern Hemisphere and the Australian region, we have compared model data from the REF-C1 hindcast run and the historical part of the REF-C2 run to observations, ERA-Interim, CCMVal-2 and CMIP5 datasets. A map of global ozone, as well as time series of October averaged Antarctic TCO, stratospheric temperature, and stratospheric winds are used to investigate the model's performance in simulating springtime ozone depletion and its stratospheric drivers and consequences. To analyse the influences of dynamical transport and chemistry on the stratosphere, model-simulated ozone and temperature vertical profiles are compared to ozonesonde data from the five sites listed in Sect. 3.5. To analyse the difference in ozone vertical profiles over the Antarctic region, vertical ClO profiles from the MLS instrument are compared for the location of Davis: 67.5–70° S, 78.75–82.5° E.

The model's ability to simulate the influence of ozone depletion on the SAM was investigated by comparing the seasonal SAM index time series with CMIP5 models and ERA-Interim data, and by comparing stratospheric zonal wind differences with ERA-Interim data. The combination of these metrics and diagnostics gives a comprehensive description of the model's improvements and differences from the CCMVal-2 ensemble and differences from observations, as well as the model's capability to simulate important metrics for Australian climate and weather.

4.1 Global ozone

Figure 1 shows zonally averaged TCO over the 2005–2010 period for the REF-C1 hindcast simulation compared to observations from the Bodeker Scientific TCO database. The yearly zonal structure of TCO compares well to observations. However, there is consistently more ozone almost globally within the REF-C1 simulation. The onset of springtime Antarctic ozone depletion occurs a little later in the REF-C1 simulation compared to the observations. This is accompanied by the maximum in ozone depletion occurring later and the persistence of ozone depletion continuing later in the year for the simulation. Despite these temporal differences, the simulated amount of ozone destroyed during the ozone hole period is similar to what is observed. The differences between REF-C1 and observations at high southern latitudes during austral winter are likely less significant due to the limited number of observations available at this time.

4.2 Historical time series

Figure 2 compares observations, the CCMVal-2 ensemble and UMUKCA-UCAM and UMUKCA-METO with the REF-C1 and REF-C2 simulations of Antarctic TCO averaged between 60–90° S for October. The latitude range of 60–90° S was chosen for the ozone comparison, as this area experiences the most significant springtime ozone depletion. The REF-C1 and REF-C2 simulations are consistently producing larger TCOs over the entire historical period examined compared to observations and the CCMVal-2 ensemble. However, the REF-C1 and REF-C2 simulations consistently lay inside the CCMVal-2 10th and 90th percentiles and have significantly smaller biases compared to UMUKCA-UCAM and UMUKCA-METO. The total amount of ozone depletion from 1960 to 2010 is also similar compared to the CCMVal-2 ensemble and observations. The inter-annual variability simulated by the model is not as large as in the observations and also, interestingly, the UMUKCA-UCAM and UMUKCA-METO models. There are also slight differences between the REF-C1 and REF-C2 simulations for the historical period. This can be attributed to the

different SST and SIC datasets used, marking the only difference between the REF-C1 and the historical part of the REF-C2 simulation before 2005.

Figure 3 similarly compares the REF-C1 and REF-C2 60–90° S averaged October temperature and 50–70° S average zonal winds to ERA-Interim, the CCMVal-2 ensemble and the UMUKCA-UCAM and UMUKCA-METO models for the stratospheric pressure levels: 100, 50 and 30 hPa. The latitude range between 50–70° S was chosen to examine the strong westerlies forming the polar vortex boundary.

At 100 hPa the REF-C1 and REF-C2 temperature simulations compare well to the ERA-Interim data, in contrast to the CCMVal-2 ensemble median, which shows a substantial cold bias of up to 6 K. The UMUKCA-UCAM and UMUKCA-METO models show a substantial warm bias at 100 hPa. The CCMVal-2 ensemble median captures a trend of decreasing temperature; consistent with colder stratospheric temperatures expected to accompany historical ozone depletion. This decreasing temperature is also seen in the REF-C1 and REF-C2 simulations, albeit to a lesser scale. The REF-C1 and REF-C2 zonal wind simulations at 100 hPa compare well with both ERA-Interim, the CCMVal-2 ensemble and UMUKCA-UCAM and UMUKCA-METO, with only slightly weaker zonal winds present in all simulations compared to ERA-Interim. This is surprising, as the cold bias present in the 100 hPa CCMVal-2 temperature is expected to be associated with more intense zonal wind, vise versa for UMUKCA-UCAM and UMUKCA-METO. However, these inconsistencies are most likely due to similar temperature gradients between the poles and mid-latitudes. The amount of variation in the REF-C1 and REF-C2 simulations is less compared to UMUKCA-UCAM and UMUKCA-METO, however does agree well with ERA-Interim.

At 50 hPa a significant cold bias exists of around 5 K in the REF-C1 and REF-C2 model runs compared to ERA-Interim data. This is not as pronounced as the CCMVal-2 ensemble median, with ACCESS-CCM being consistently 3 K warmer after 1970. Note the ERA-Interim data still mostly lay within the 10th and 90th percentiles of the CCMVal-2 ensemble (illustrating large inter-model variability). The differences between the CCMVal-2 ensemble and the REF-C1 and REF-C2 simulations is likely associated with the larger ozone concentration present in the ACCESS-CCM model compared to the CCMVal-2 ensemble, as

a higher ozone concentration warms the stratosphere through more absorption of UV radiation. The UMUKCA-UCAM and UMUKCA-METO models agree reasonably well with the ERA-Interim data at 50 hPa in both amount and variability. A slight decreasing temperature trend is simulated over the historical period, which is not as pronounced as in the CCMVal-2 ensemble. At 50 hPa there is an intensification of the polar vortex due to colder 50 hPa temperatures in the CCMVal-2 ensemble, however, the REF-C1 and REF-C2 simulations still agree well with ERA-Interim values. The UMUKCA-UCAM and UMUKCA-METO zonal winds are slightly weaker compared to ACCESS-CCM, but with variation closer to observations. The differences between the CCMVal-2 ensemble median and the REF-C1 and REF-C2 simulations increase with time, reaching a maximum of 5 ms^{-1} at year 2000, and are reflective of the temperature differences.

At 30 hPa, the REF-C1 and REF-C2 simulations of temperature follow the CCMVal-2 ensemble median closely, with a large cold temperature bias relative to ERA-Interim, of 10–15 K. However, again the ERA-Interim mostly lay within CCMVal-2 inter-model variability (10th and 90th percentiles). This cold bias is accompanied by slightly stronger zonal winds in the REF-C1 and REF-C2 simulations compared to ERA-Interim. The large cold biases seen at 50 and 30 hPa may be due to reduced heat flux in the model compared to ERA-Interim (not shown). A possible cause of the reduced heat flux could be the coarse resolution of the model inadequately representing fine-scale structure (e.g. Austin et al. (2003)). An even stronger zonal wind is associated with the CCMVal-2 ensemble, with a maximum difference of 5 ms^{-1}. The increasing trend in the polar vortex strength seen in the CCMVal-2 models is not as pronounced in the REF-C1 and REF-C2 simulations. Also, UMUKCA-UCAM and UMUKCA-METO simulate 30 hPa temperatures and variation well compared to ERA-Interim, with a slightly weaker climatological polar vortex.

Overall, ACCESS-CCM, with the updated HadGEM3 background climate model, shows better representation of Antarctic October TCO, stratospheric zonal wind and 100 hPa temperatures compared to UMUKCA-UCAM and UMUKCA-METO. However, stratospheric temperatures below 50 hPa show a substantial cold bias that is not seen in UMUKCA-UCAM and UMUKCA-METO. Compared to the CCMVal-2 ensemble, ACCESS-CCM is simulating

stratospheric temperatures and zonal winds more accurately, with only the small trade off of slightly enhanced TCO. UMUKCA-UCAM and UMUKCA-METO also represent variation more accurately compared to ACCESS-CCM.

4.3 Ozone, temperature and ClO profiles

Figure 4 shows vertical ozone profiles seasonally averaged over 2005–2010 for the REF-C1 simulation compared to ozonesonde observations for five Southern Hemisphere sites and their nearest coincident model grid box. Similarly, Fig. 5 shows vertical temperature profiles averaged over the same time period and locations. To highlight the variability, shaded regions show one standard deviation of the monthly averaged model output for the REF-C1 profiles and one standard deviation divided by $\sqrt{7.5}$ for the ozonesonde profiles. The ozonesonde standard deviations are divided by $\sqrt{7.5}$ for visualisation purposes. We have presumed an average of one sounding per week, therefore, with the assumption of normal statistics, this will approximate the standard deviation of a monthly average, consistent with the model data used. The differences between the two datasets for both ozone concentration and temperature are also provided between 200–10 hPa. Anomalies are visibly present in the upper levels of ozonesonde measurements, particularly in the temperature profiles. At these levels measurement sample size is severely reduced, resulting in possible skewed seasonal averages.

Figures 4 and 5 illustrate that there is general agreement in both ozone and temperature profiles between the ozonesondes and the REF-C1 simulation for Melbourne. The location of the peak in ozone concentration is consistent between REF-C1 and ozonesondes throughout summer, autumn and winter. There is a slight difference during spring, with the model simulating a slightly higher ozone peak altitude relative to ozonesondes. Consistently the model simulates excessive ozone peak concentrations between 20 and 25 km. This is largest for autumn, with an excess of 8 % simulated by the model. Above 100 hPa there are consistent cold biases of up to 3 K that extend up to 10 hPa during all seasons, especially during summer and autumn. There is also a warm bias in all seasons centered near 100 hPa.

The comparison at Lauder and Macquarie Island illustrates poorer agreement between the REF-C1 simulation and ozonesonde ozone observations. The ozone concentration peak altitudes are still consistent between the datasets, with the largest exception at Macquarie during summer, where the REF-C1 profile peak is situated slightly higher. Again, the model is predicting excess ozone concentration peaks during all seasons, with the largest at Lauder of 20 % during summer, and at Macquarie of 20 % during winter. The REF-C1 temperature profiles generally agree well with ozonesondes. However, there is still a cold bias present above 100 hPa in all seasons except winter at Lauder. The cold bias is as large as 4 K during summer at Lauder. There is also a cold bias of 4 and 6 K at Macquarie near the tropopause at 170 hPa during winter and spring respectively.

Davis (located within the polar vortex collar region) comparisons of REF-C1 and ozonesonde profiles show very significant differences. During summer, spring, and autumn the simulated ozone maximum is at consistently higher altitudes compared to ozonesondes. The model is also simulating significantly more ozone during autumn and winter, with an excess of 26 % in maximum ozone concentration during winter. Simulated summer and to a lesser extent, autumn, temperature profiles also show a cold temperature bias, most noticeable between 200 and 30 hPa. Here, the REF-C1 simulations show colder temperatures of over 6 K near 50 hPa during summer. The winter simulated temperature profile agrees very well with ozonesondes, in contrast to ozone concentrations, where there is a very large difference. Davis is located in an area that experiences perturbed springtime polar ozone depletion. Here, ozone depletion is captured in the simulated ozone profiles mostly between 50 and 20 hPa. This is in contrast to what is observed by ozonesonde profiles, where the majority of ozone depletion is seen at a lower altitude, below 50 hPa and centered around 100 hPa. This indicates a clear inadequacy of the model in capturing the springtime vertical ozone structure. The simulated temperature profiles at Davis also show a large cold bias above 50 hPa of up to 11 K, associated with the altitude of ozone depletion in the model. Accompanying this is a model warm bias below 50 hPa, centered at 100 hPa, of up to 5 K. The variability, seen in the standard deviations is also much larger during spring for ozonesondes and REF-C1 compared to other seasons. This is due to the variable

nature of springtime Antarctic ozone depletion, and the location of Davis, which is often in the collar region of the polar vortex.

Due to the dynamical variability experienced by Davis, with Davis being in the polar vortex edge region, comparisons of simulated and ozonesonde vertical ozone concentration and temperature for the South Pole were conducted. The South Pole shows very similar differences between ozonesondes and REF-C1 model simulations for both ozone concentrations and temperature to Davis. Therefore the disparity in the vertical location of springtime ozone depletion seen at Davis is not due to its potential location on the edge of the polar vortex. However, there are some differences. The amount of ozone depletion simulated during spring in the model is now enhanced greatly, with almost all ozone destroyed above 50 hPa. While ozonesondes only show slightly more ozone depletion. The discrepancy in the altitude of significant ozone depletion is still present, with the model simulating ozone depletion much higher than is observed. This produces a more pronounced cold bias in the model above 50 hPa with differences reaching 15 K at 30 hPa during spring. The 100 hPa warm bias is not as pronounced compared to Davis at approximately 3 K.

A consistent ozone excess at all stations during seasons that are not perturbed by springtime ozone loss is seen in the vertical ozone profiles, increasing with increasing latitude (Fig. 4). This suggests possible problems with transport in the model. Also, as the model shows excess ozone globally, cold biases above 10 hPa may also be affecting gas phase ozone chemical cycles. On a global average scale, the stratospheric cold biases simulated by the model are likely due to incorrect concentrations and distributions of radiatively active gases or problems with the radiative scheme (SPARC-CCMVal, 2010). The two main radiative gases that are tied into the chemistry scheme in the stratosphere are ozone and water vapour. Global water vapour distributions of a previous iteration of this model where analysed in Morgenstern et al. (2009) and where shown to agree well with ERA-40 climatology.

Apart from any systematic biases, such as due to the coarse resolution of the model, the large differences seen in the vertical structure of perturbed springtime ozone between the REF-C1 simulation and ozonesondes are either chemical or dynamical in nature, or some combination of both. The slightly colder winter temperatures seen in the model over

Antarctic regions can have implications for PSC formation and are likely a result of less pole-ward heat transport, analysed through comparison of 45–75° S heat flux with MERRA reanalysis (not shown). To investigate the links between the chemistry and dynamics of the problem, Fig. 6 shows a comparison of ClO volume mixing ratio, extracted for the region of 67.5–70° S, 78.75–82.5° E corresponding to Davis and temporally averaged between 2005–2010 for the REF-C1 simulation and MLS satellite observations. Only 3 pm (local solar time) values from MLS are used in the average. The REF-C1 averages were produced using instantaneous 3 hourly output, with the closest coincident time to 3 pm used, corresponding to approximately 2 pm at Davis. Only 3 pm values were used as ClO has a strong diurnal cycle, with concentrations peaking during sunlit hours. This ensures the model averages represent the ClO observations. The altitude of large ClO volume mixing ratios is an indication of the altitude of where chemical cycles that are responsible for the destruction of ozone are occurring. The slight differences in local solar times used may result in a small disparity in amount of ClO. However, by taking a seasonal average, we expect this to be small. The aim of this comparison is to highlight any differences in the vertical locations of ClO volume mixing ratios, thus providing an indication of where the ozone loss chemical reactions are taking place.

During summer and autumn, the structure and peak of the simulated ClO profiles agrees very well with MLS measurements, with only slightly larger volume mixing ratios in the REF-C1 simulation. The winter profiles show very good agreement of the ClO peak location below 5 hPa. A minimum is seen near 10 hPa, agreeing well with MLS, while a maximum is located near 20 hPa, also agreeing well with MLS. However, the amount of ClO in the REF-C1 simulation is markedly larger compared to MLS. Above 5 hPa the ClO peak in REF-C1 is lower compared to MLS, at about 35 km compared to 40 km. There is a large difference between the REF-C1 simulated ClO and that observed by MLS during spring. A peak is seen near 50 hPa in both REF-C1 and MLS. However, above 50 hPa, ClO in REF-C1 stays consistently larger compared to MLS up to 5 hPa, indicating that ClO is alot more active at higher altitudes compared to MLS. Below 50 hPa, ClO in REF-C1 decreases rapidly compared to MLS with MLS ClO volume mixing ratios larger below 100 hPa. Also,

similar to winter, the ClO peak at upper altitudes is occurring around 5 km lower in ERF-C1, at 35 km, compared to 40 km in MLS. These ClO observations are consistent with the vertical structure of springtime ozone concentrations, and that our model misrepresents the altitude of ozone depletion over Davis and the South Pole.

These results suggest the colder Antarctic stratospheric temperatures above 50 hPa seen in the model are causing enhanced PSC formation at higher altitudes, and thus more heterogeneous reactions on the surface of PSCs. This is indeed the case through analysis of simulated nitric acid trihydrate (NAT) PSCs (not shown), which show persistent upper level (25 km and higher) PSCs throughout winter. Winter temperature profiles at the South Pole show a slight cold bias, agreeing well with the enhancement of PSCs at these levels, and perhaps indicating reduced sedimentation. This is further highlighted by the disparity in MLS measured and modelled ClO springtime profiles, with REF-C1 showing consistent ClO volume mixing ratios above 50 hPa due to due to heterogeneous reactions on PSCs. There is also absence of a well defined minimum in the modelled springtime ClO profile as seen around 20 hPa in MLS measurements. This agrees well with the large differences seen in the vertical location of ozone depletion simulated for Davis and the South Pole, consistent with the large springtime cold biases present in the model at 50 and 30 hPa. The lack of ozone depletion at lower altitude compared to ozonesondes, and sharp decline in ClO volume mixing ratios could possible be explained by the absence of STS simulated by the model due to their higher effectiveness at lower altitudes (Solomon, 1999). The amount of ozone depletion at lower altitudes will also be influenced by the warm model bias, which will affect the strongly temperature dependent heterogeneous chemistry.

4.4 Southern annular mode

Figure 7 shows Southern Hemisphere seasonal SAM indices for REF-C1 and the historical part of REF-C2 compared to ERA-Interim data from 1979–2010 and the recent past section of the historical simulations from CMIP5 runs that used prescribed ozone (Eyring et al., 2013a). The seasonal SAM index was calculated following Morgenstern et al. (2014), using the seasonally averaged difference in area-averaged surface pressure between 38.75–

61.25° S and 63.75–90° S. To be able to appropriately compare to ERA-Interim and CMIP5 data, this value was normalised by subtracting the 1979–2005 mean of the calculated SAM indices. The REF-C1, REF-C2 and ERA-Interim seasonal SAM indices are shown as both the yearly seasonal average (highlighting the year-to-year variability) and also as a ten-year running mean (highlighting the comparison to the CMIP5 ensemble). The CMIP5 time series shows the ensemble median and the 10th and 90th percentiles interval of the ensemble range.

During summer the CMIP5 ensemble captures a noticeable increase in the SAM index between 1960–2005, consistent with historical Antarctic ozone depletion. A large range in the ensemble data seen in the 10th and 90th percentiles accompanies this. The REF-C1 and REF-C2 data also agree well with the CMIP5 ensemble median, showing an increase in the simulated SAM index. There is a large amount of year-to-year variability in the REF-C1 and REF-C2 time-series, which mostly lay within the CMIP5 10th and 90th percentiles and very similar to what is seen in the ERA-Interim data. There are also noticeable differences between the REF-C1 and REF-C2 data, mostly before 1985. This can be mostly attributed to different SSTs and the SICs used between the two model runs, or random climate fluctuations. The differences in temporal Antarctic stratospheric ozone depletion between the REF-C1 and REF-C2 would also be an important influence. The increasing SAM index is representative of a southward shift of the westerly winds and precipitation regimes, and is attributed to both decreasing Antarctic stratospheric ozone concentrations and increasing GHGs. An increasing summer SAM index simulated by the model not only agrees with CMIP5 data and ERA-Interim re-analysis, it also complements conclusions from Keeble et al. (2014), which show significant increases in SAM attributed to lower stratospheric ozone depletion within a similar model environment.

Autumn also shows an increase in the SAM index in the CMIP5 ensemble, albeit on a smaller scale to that seen in summer. The REF-C1 and REF-C2 time-series agree well with the CMIP5 data and especially well with the ERA-Interim data. An increase in the SAM index over time is consistent with the CMIP5 ensemble, and the year-to-year variability of the REF-C1 time-series is consistently within the CMIP5 10th and 90th percentiles. How-

ever, the REF-C2 seasonal variation shows a frequent low SAM index values outside of the CMIP5 variability, most frequently before 1980. The cause of the positive SAM trend observed during autumn is currently not well understood (Canziani et al., 2014). The seasonal variation seen in the REF-C1 and REF-C2 time-series is also similar to that seen in the ERA-Interim data. The differences between the REF-C1 and REF-C2 time-series are much less pronounced, especially after 1980 where they follow each other closely. The differences before 1980 can be attributed to the different SSTs and SICs used or random climate fluctuations, and less likely due to the differences in stratospheric ozone.

The winter and spring SAM indexes are consistent between all datasets over the entire time-series. There is no noticeable long-term change in the CMIP5 ensemble, with the REF-C1 and REF-C2 time series agreeing well. The largest excursion from the CMIP5 ensemble median is seen in the REF-C2 time-series centered around 1970 during winter, where a positive SAM index is seen consistently over 3 years. A noticeable difference between the REF-C1 and REF-C2 winter and spring SAM indexes is a strong decadal correlation during spring, in contrast to the winter comparison.

With the current model setup, we cannot completely distinguish between the influences from stratospheric ozone changes, GHGs, and the prescribed SSTs and SICs. It is clear that the REF-C1 and REF-C2 simulations are distinct from each other, with the only major difference in the simulation setups being different SSTs and SICs. This indicates that SSTs and SICs are having a noticeable influence. However, the influence from stratospheric ozone has been captured in a sensitivity simulation with fixed GHGs, SSTs and SICs at 1960 levels. This simulation (not shown), shows a clear influence from ozone on the SAM, indicating that the increasing trend in the summer SAM shown here is influenced significantly by ozone.

South East Australia is likely to experience a higher probability of rainfall due to a positive SAM trend during summer. This is due to a southward shift of the westerly winds resulting in more prominent easterlies over this region, enhancing orographic driven rainfall (e.g. Thompson et al. (2011)). However, the slight increase in the SAM seen during autumn in all

datasets will have a different effect, as in this case, a southward shift of the westerly winds will decrease the penetration of cold fronts northwards.

4.5 Zonal wind anomalies

Figure 8 shows 50 hPa average zonal winds of 1979–1988 minus the 2001–2010 average for REF-C1, REF-C2, and ERA-Interim data for the months of August, October and December. The ten-year averages represent the earliest time available in the ERA-Interim and the latest time available in the historical simulations, while also being able to represent important phases in stratospheric springtime Antarctic ozone depletion, with 1979–1988 representing the onset of ozone depletion while 2001–2010 representing the maximum springtime ozone depletion. The months of August, October and December where chosen to represent different stages of the annually forming ozone hole. The ozone hole typically begins forming in late August, reaching a maximum by the end of October, and closing by mid-December.

August shows some small-scale differences between the REF-C1 and REF-C2 relative to ERA-Interim, most likely caused by differences in decadal variations between the model and observations. October shows some larger differences, with an opposite dipole in the western hemisphere when comparing REF-C1 and REF-C2 with ERA-Interim. Again, this can be attributed to decadal differences in the variations, and possible differences in the maximum location in zonal wind, which is more pole-ward in ERA-Interim compared to the model simulations. The December differences are very consistent across the REF-C1, REF-C2, and ERA-Interim data, with increasing zonal wind seen south of 60° S. This is an indication of the strengthening of the polar vortex due to Antarctic ozone depletion, and is consistent with the increasing summertime SAM index seen in the ERA-Interim and model simulations.

5 Conclusions

The ACCESS-CCM model presented here is able to confidently provide an initial contribution from Australia to the international community via the Chemistry-Climate Model Initiative (CCMI). It simulates slightly larger October total column ozone values compared to observations and the CCMVal-2 ensemble, however simulates a similar ozone decline over the historical period (1960 to 2010). A cold bias compared to ERA-Interim of up to 5 K at 50 hPa and 10–15 K at 30 hPa is present during October. This is an improvement from the CCMVal-2 ensemble, which shows colder temperatures compared to ACCESS-CCM at 100 and 50 hPa of up to of 5 and 3 K respectively. Our model simulates polar vortex strength above 100 hPa closer to ERA-Interim compared to the CCMVal-2 ensemble median. Compared to the UMUKCA models, ACCESS-CCM is simulating TCO, 50 and 30 hPa zonal wind and 100 hPa temperature more accurately. However, the 50 and 30 hPa ACCESS-CCM cold bias is not present in the UMUKCA models. This indicates that even with the vast improvements in ACCESS-CCM compared to its precursors, there are still are still some problems in the model.

Model-simulated seasonal averaged vertical profiles of ozone and temperature compared to Southern Hemisphere ozonesondes show very good agreement in ozone vertical distribution, concentration and seasonal variation for Melbourne, with only a small excess ozone bias in ACCESS-CCM. However, there is less agreement at higher latitudes sites, with peak ozone concentrations in larger excess of observed values. The largest difference outside the perturbed springtime conditions is seen at Davis and the South Pole during winter, with ACCESS-CCM simulating in excess of 26%. A stratospheric cold bias is also present outside perturbed springtime conditions, most noticeably over polar latitudes during summer and autumn of up to 10 K at 50 and 200 hPa respectively. The majority of springtime ozone depletion at Davis and the South Pole is occurring above 50 hPa in ACCESS-CCM compared to being centered near 100 hPa in ozonesondes. This is also accompanied by a significant cold bias in the stratosphere during spring at the altitudes of ozone depletion in the model.

The altitude differences of springtime polar ozone loss can be attributed to differences in simulated ClO profiles during spring, pointing to a modelling deficiency in simulating heterogeneous chlorine release. The MLS instrument shows a peak in ClO at and below 50 hPa and a well defined minimum at 20 hPa. ACCESS-CCM instead shows consistent ClO above the 50 hPa peak. This can be explained by the simulation of colder stratospheric temperatures, possibly caused by reduced mid-latitude heat flux, enhancing PSC formation at these altitudes, and thus providing a mechanism for increased ozone loss at higher altitudes. The deficiency in modelling large springtime ClO volume mixing ratios below 100 hPa, explains the relatively small simulated ozone loss at these altitudes relative to ozonesonde observations, and could possible be due to the models inability simulating supercooled ternary solution polar stratospheric clouds and the higher model temperatures simulated there.

The large model-ozonesonde differences in the ozone profiles during summer, autumn and winter, seasons outside perturbed polar springtime ozone loss conditions, is consistent with the excess ozone seen in the global total column ozone map (Fig. 1), and time series (Fig. 2). This could possibly be due to too much transport in the model, and cold biases above 10 hPa affecting the gas-phase ozone chemical cycles. The drivers of the cold biases and excessive transport within the ACCESS-CCM are unclear, however, mid-latitude cold biases are likely influenced by incorrect radiatively active gases such as ozone and water vapour or inaccuracies in the radiation scheme. Whereas lower simulated mid-latitude heat flux is likely a driver of the high latitude cold biases.

The SAM index for ACCESS-CCM agrees well with ERA-Interim and CMIP5 ensemble. All show an increasing SAM index during summer and to a lesser extent autumn, indicating a southward shift of mid-latitude winds and storm tracks. Zonal wind differences of 1979–1988 average minus 2001–2010 average at 50 hPa during December show increasing high south latitude wind strength, consistent with the simulated increase in the SAM during summer, important for properly simulating Australian climate.

Future versions of this model will follow the UKCA release candidates, with a major goal of obtaining a fully coupled chemistry-climate-ocean model.

Acknowledgements. This work was supported through funding by the Australian Government's Australian Antarctic Science Grant Program (FoRCES 4012), the Australian Research Council's Centre of Excellence for Climate System Science (CE110001028), the Commonwealth Department of the Environment (grant 2011/16853), and NIWA as part of its New Zealand Government-funded, core research, and by the Marsden Fund Council from Government funding, administered by the Royal Society of New Zealand (grant 12-NIW-006). This research was undertaken with the assistance of resources provided at the NCI National Facility systems at the Australian National University through the National Computational Merit Allocation Scheme supported by the Australian Government. The authors wish to thank all past ozonesonde observers. All data used in this paper can be downloaded from the CCMI web portal (http://www.met.reading.ac.uk/ccmi/) or obtained from the lead author. We acknowledge the UK Met Office for use of the MetUM.

References

Arblaster, J. M. and Meehl, G. A.: Contributions of external forcings to southern annular mode trends, J. Climate, 19, 2896–2905, doi:10.1175/JCLI3774.1, 2006.

Arblaster, J. M., Meehl, G. A., and Karoly, D. J.: Future climate change in the Southern Hemisphere: competing effects of ozone and greenhouse gases, Geophys. Res. Lett., 38, L02701, doi:10.1029/2010GL045384, 2011.

Arblaster, J. M. and Gillett, N. P.: Stratospheric ozone changes and climate, Chapter 4 in *Scientific Assessment of Ozone Depletion: 2014*, Global Ozone Research and Monitoring Project–Report No. 55, World Meteorological Organization, Geneva, Switzerland, 2014.

Archibald, A. T., Levine, J. G., and Abraham, N. L.: Impacts of HO_x regeneration and recycling in the oxidation of isoprene: consequences for the composition of past, present and future atmospheres, Geophys. Res. Lett., 38, L05804, doi:10.1029/2010GL046520, 2011.

Austin, J., Shindell, D., Beagley, S. R., Brühl, C., Dameris, M., Manzini, E., Nagashima, T., Newman, P., Pawson, S., Pitari, G., Rozanov, E., Schnadt, C., and Shepherd, T. G.: Uncertainties and assessments of chemistry-climate models of the stratosphere, Atmos. Chem. Phys., 3, 1–27, doi:10.5194/acp-3-1-2003, 2003.

Austin, J., Scinocca, J., Plummer, D., Oman, L., Waugh, D., Akiyoshi, H., Bekki, S., Braesicke, P., Butchart, N., Chipperfield, M., Cugnet, D., Dameris, M., Dhomse, S., Eyring, V., Frith, S., Garcia, R. R., Garny, H., Gettelman, A., Hardiman, S. C., Kinnison, D., Lamarque, J. F., Mancini, E.,

Marchand, M., Michou, M., Morgenstern, O., Nakamura, T., Pawson, S., Pitari, G., Pyle, J., Rozanov, E., Shepherd, T. G., Shibata, K., Teyssèdre, H., Wilson, R. J., and Yamashita, Y.: Decline and recovery of total column ozone using a multimodel time series analysis, J. Geophys. Res., 115, D00M10, doi:10.1029/2010JD013857, 2010.

Banerjee, A., Archibald, A. T., Maycock, A. C., Telford, P., Abraham, N. L., Yang, X., Braesicke, P., and Pyle, J. A.: Lightning NO_x, a key chemistry–climate interaction: impacts of future climate change and consequences for tropospheric oxidising capacity, Atmos. Chem. Phys., 14, 9871–9881, doi:10.5194/acp-14-9871-2014, 2014.

Barnett, J. J., Houghton, J. T., and Pyle, J. A.: The temperature dependence of the ozone concentration near the stratopause, Q.J. Roy. Meteor. Soc., 101, 245–257, doi:10.1002/qj.49710142808, 1975.

Bian, H., and Prather, M. J.: Fast-J2: Accurate Simulation of Stratospheric Photolysis in Global Chemical Models, J. Atmos. Chem., 41, 281–296, doi:10.1023/A:1014980619462, 2002.

Bodeker, G. E., Shiona, H., and Eskes, H.: Indicators of Antarctic ozone depletion, Atmos. Chem. Phys., 5, 2603–2615, doi:10.5194/acp-5-2603-2005, 2005.

Butchart, N., Scaife, A. A., Bourqui, M., and De Grandpre, J.: Simulations of anthropogenic change in the strength of the Brewer–Dobson circulation, Clim. Dynam., 27, 727–741, doi:10.1007/s00382-006-0162-4, 2006.

Canziani, P. O., O'Neill, A., Schofield, R., Raphael, M., Marshall, G. J., and Redaelli, G.: World climate research programme special workshop on climatic effects of ozone depletion in the Southern Hemisphere, B. Am. Meteorol. Soc., 95, ES101–ES105, doi:10.1175/BAMS-D-13-00143.1, 2014.

Dameris, M., Godin-Beekmann, S., Alexander, S., Braesicke, P., Chipperfield, M., de Laat, A. T. J., Orsolini, Y., Rex, M., and Santee, M. L.: Update on Polar ozone: past, present, and future, in: Chapter 3 in Scientific Assessment of Ozone Depletion: 2014, Global Ozone Research and Monitoring Project, Report No. 55, World Meteorological Organization, Geneva, Switzerland, 2014.

Davies, T., Cullen, M., and Malcolm, A. J.: A new dynamical core for the Met Office's global and regional modelling of the atmosphere, Q. J. Roy. Meteor. Soc., 131, 1759–1782, doi:10.1256/qj.04.101, 2005.

Dee, D. P., Uppala, S. M., Simmons, A. J., Berrisford, P., Poli, P., Kobayashi, S., Andrae, U., Balmaseda, M. A., Balsamo, G., Bauer, P., Bechtold, P., Beljaars, A. C. M., van de Berg, L., Bidlot, J., Bormann, N., Delsol, C., Dragani, R., Fuentes, M., Geer, A. J., Haimberger, L., Healy, S. B., Hersbach, H., Hólm, E. V., Isaksen, L., Kållberg, P., Köhler, M., Matricardi, M., McNally, A. P., Monge-Sanz, B. M., Morcrette, J. J., Park, B. K., Peubey, C., de Rosnay, P., Tavolato, C., Thé-

paut, J. N., and Vitart, F.: The ERA-Interim reanalysis: configuration and performance of the data assimilation system, Q. J. Roy. Meteor. Soc., 137, 553–597, doi:10.1002/qj.828, 2011.

de Laat, A. T. M., van der A, R. J., van Weele, M.: Tracing the second stage of ozone recovery in the Antarctic ozone-hole with a "big data" approach to multivariate regressions, Atmos. Chem. Phys., 15, 79–97, doi:10.5194/acp-15-79-2015, 2015.

Edwards, J. M. and Slingo, A.: Studies with a flexible new radiation code. I: Choosing a configuration for a large-scale model , Q. J. Roy. Meteor. Soc., 122, 689–719, doi:10.1002/qj.49712253107, 1996.

Eyring, V., Arblaster, J. M., and Cionni, I.: Long-term ozone changes and associated climate impacts in CMIP5 simulations, J. Geophys. Res., 118, 5029–5060, doi:10.1002/jgrd.50316, 2013a.

Eyring, V., Lamarque, J.-F., Hess, P., Arfeuille, F., Bowman, K., Chipperfiel, M. P., Duncan, B., Fiore, A., Gettelman, A., Giorgetta, M. A., Granier, C., Hegglin, M., Kinnison, D., Kunze, M., Langematz, U., Luo, B., Martin, R., Matthes, K., Newman, P. A., Peter, T., Robock, A., Ryerson, T., Saiz-Lopez, A., Salawitch, R., Schultz, M., Shepherd, T. G., Shindell, D., Staehelin, J., Tegtmeier, S., Thomason, L., Tilmes, S., Vernier, J.-P., Waugh, D., and Young, P. Y.: Overview of IGAC/SPARC Chemistry-Climate Model Initiative (CCMI) community simulations in support of upcoming ozone and climate assessments, SPARC Newsletter, 40, 48–66, 2013b.

Gillett, N. P. and Thompson, D. W. J.: Simulation of recent Southern Hemisphere climate change, Science, 302, 273–275, doi:10.1126/science.1087440, 2003.

Granier, C., Bessagnet, B., Bond, T., D'Angiola, A., Denier van der Gon, H., Frost, G. J., Heil, A., Kaiser, J. W., Kinne, S., Klimont, Z., Kloster, S., Lamarque, J.-F., Liousse, C., Masui, T., Meleux, F., Mieville, A., Ohara, T., Raut, J.-C., Riahi, K., Schultz, M. G., Smith, S. J., Thompson, A., van Aardenne, J., van der Werf, G. R., and van Vuuren, D. P.: Evolution of anthropogenic and biomass burning emissions of air pollutants at global and regional scales during the 1980–2010 period, Climatic Change, 109, 163–190, doi:10.1007/s10584-011-0154-1, 2011.

Hewitt, H. T., Copsey, D., Culverwell, I. D., Harris, C. M., Hill, R. S. R., Keen, A. B., McLaren, A. J., and Hunke, E. C.: Design and implementation of the infrastructure of HadGEM3: the next-generation Met Office climate modelling system, Geosci. Model Dev., 4, 223–253, doi:10.5194/gmd-4-223-2011, 2011.

Jones, C. D., Hughes, J. K., Bellouin, N., Hardiman, S. C., Jones, G. S., Knight, J., Liddicoat, S., O'Connor, F. M., Andres, R. J., Bell, C., Boo, K.-O., Bozzo, A., Butchart, N., Cadule, P., Corbin, K. D., Doutriaux-Boucher, M., Friedlingstein, P., Gornall, J., Gray, L., Halloran, P. R., Hurtt, G., Ingram, W. J., Lamarque, J.-F., Law, R. M., Meinshausen, M., Osprey, S., Palin, E. J.,

Parsons Chini, L., Raddatz, T., Sanderson, M. G., Sellar, A. A., Schurer, A., Valdes, P., Wood, N., Woodward, S., Yoshioka, M., and Zerroukat, M.: The HadGEM2-ES implementation of CMIP5 centennial simulations, Geosci. Model Dev., 4, 543–570, doi:10.5194/gmd-4-543-2011, 2011.

Jonsson, A. I., De Grandpre, J., and Fomichev, V. I.: Doubled CO_2-induced cooling in the middle atmosphere: photochemical analysis of the ozone radiative feedback, J. Geophys. Res., 109, D24103, doi:10.1029/2004JD005093, 2004.

Keeble, J., Braesicke, P., Abraham, N. L., Roscoe, H. K., and Pyle, J. A.: The impact of polar stratospheric ozone loss on Southern Hemisphere stratospheric circulation and climate, Atmos. Chem. Phys., 14, 13705–13717, doi:10.5194/acp-14-13705-2014, 2014.

Lamarque, J. F., Kyle, G. P., Meinshausen, M., and Riahi, K.: Global and regional evolution of short-lived radiatively-active gases and aerosols in the Representative Concentration Pathways, Climatic Change, 109, 191–212, doi:10.1007/s10584-011-0155-0, 2011.

Lamarque, J.-F., Shindell, D. T., Josse, B., Young, P. J., Cionni, I., Eyring, V., Bergmann, D., Cameron-Smith, P., Collins, W. J., Doherty, R., Dalsoren, S., Faluvegi, G., Folberth, G., Ghan, S. J., Horowitz, L. W., Lee, Y. H., MacKenzie, I. A., Nagashima, T., Naik, V., Plummer, D., Righi, M., Rumbold, S. T., Schulz, M., Skeie, R. B., Stevenson, D. S., Strode, S., Sudo, K., Szopa, S., Voulgarakis, A., and Zeng, G.: The Atmospheric Chemistry and Climate Model Intercomparison Project (ACCMIP): overview and description of models, simulations and climate diagnostics, Geosci. Model Dev., 6, 179–206, doi:10.5194/gmd-6-179-2013, 2013.

Li, F., Stolarski, R. S., and Newman, P. A.: Stratospheric ozone in the post-CFC era, Atmos. Chem. Phys., 9, 2207–2213, doi:10.5194/acp-9-2207-2009, 2009.

Livesey, N. J., Read, W. G., Froidevaux, L., Lambert, A., Manney, G. L., Pumphrey, H. C., Santee, M. L., Schwartz, M. J., Wang, S., and Cofield, R. E.: Version 3.3 Level 2 data quality and description document, Jet Propulsion Laboratory, California Institute of Technology, Pasadena, California, D-33509, 2011.

Meinshausen, M., Smith, S. J., Calvin, K., Daniel, J. S., Kainuma, M. L. T., Lamarque, J. F., Matsumoto, K., Montzka, S. A., Raper, S. C. B., Riahi, K., Thomson, A., Velders, G. J. M., and Vuuren, D. P. P.: The RCP greenhouse gas concentrations and their extensions from 1765 to 2300, Climatic Change, 109, 213–241, doi:10.1007/s10584-011-0156-z, 2011.

Morgenstern, O., Braesicke, P., O'Connor, F. M., Bushell, A. C., Johnson, C. E., Osprey, S. M., and Pyle, J. A.: Evaluation of the new UKCA climate-composition model – Part 1: The stratosphere, Geosci. Model Dev., 2, 43–57, doi:10.5194/gmd-2-43-2009, 2009.

Morgenstern, O., Zeng, G., Luke Abraham, N., Telford, P. J., Braesicke, P., Pyle, J. A., Hardiman, S. C., O'Connor, F. M., and Johnson, C. E.: Impacts of climate change, ozone recovery, and increasing methane on surface ozone and the tropospheric oxidizing capacity, J. Geophys. Res.-Atmos., 118, 1028–1041, doi:10.1029/2012JD018382, 2013.

Morgenstern, O., Zeng, G., and Dean, S. M.: Direct and ozone-mediated forcing of the Southern Annular Mode by greenhouse gases, Geophys. Res. Lett., 41, 9050–9057, doi:10.1002/2014GL062140, 2014.

Müller, R., Grooß, J. -U., Heinze, D., Dameris, M., abd Bodeker, G.: Simple measures of ozone depletion in the polar stratosphere, J. Geophys. Res., 8, 251–264, doi:10.5194/acp-8-251-2008, 2008.

Neu, J. L., Prather, M. J., and Penner, J. E.: Global atmospheric chemistry: integrating over fractional cloud cover, J. Geophys. Res., 112, D11306, doi:10.1029/2006JD008007, 2007.

O'Connor, F. M., Johnson, C. E., Morgenstern, O., Abraham, N. L., Braesicke, P., Dalvi, M., Folberth, G. A., Sanderson, M. G., Telford, P. J., Voulgarakis, A., Young, P. J., Zeng, G., Collins, W. J., and Pyle, J. A.: Evaluation of the new UKCA climate-composition model – Part 2: The Troposphere, Geosci. Model Dev., 7, 41–91, doi:10.5194/gmd-7-41-2014, 2014.

Priestley, A.: A quasi-conservative version of the semi-Lagrangian advection scheme, Mon. Weather Rev., 121, 621–629, doi:10.1175/1520-0493(1993)121<0621:AQCVOT>2.0.CO;2, 1993.

Rayner, N. A., Parker, D. E., and Horton, E. B.: Global analyses of sea surface temperature, sea ice, and night marine air temperature since the late nineteenth century, J. Geophys. Res., 108, 4407, doi:10.1029/2002JD002670, 2003.

Riahi, K., Rao, S., Krey, V., Cho, C., Chirkov, V., Fischer, G., Kindermann, G., Nakicenovic, N., and Rafaj, P.: RCP 8.5 – a scenario of comparatively high greenhouse gas emissions, Climatic Change, 109, 33–57, doi:10.1007/s10584-011-0149-y, 2011.

Santee, M. L., Lambert, A., and Read, W. G.: Validation of the Aura Microwave Limb Sounder ClO measurements, J. Geophys. Res., 113, D15S22, doi:10.1029/2007JD008762, 2008.

Scaife, A. A., Butchart, N., Warner, C. D., and Swinbank, R.: Impact of a spectral gravity wave parameterization on the stratosphere in the met office unified model, J. Atmos. Sci., 59, 1473–1489, doi:10.1175/1520-0469(2002)059<1473:IOASGW>2.0.CO;2, 2002.

Schultz, M. G., Heil, A., and Hoelzemann, J. J.: Global wildland fire emissions from 1960 to 2000, Global Biogeochem. Cy., 22, GB2002, doi:10.1029/2007GB003031, 2008.

Shepherd, T. G.: Dynamics, stratospheric ozone, and climate change, Atmos. Ocean, 46, 117–138, doi:10.3137/ao.460106, 2008.

Shepherd, T. G., Plummer, D. A., Scinocca, J. F., Hegglin, M. I., Fioletov, V. E., Reader, M. C., Remsberg, E., von Clarmann, T., Wang, H. J.: Reconciliation of halogen-induced ozone loss with the total-column ozone record, Nature Geosci., 7, 443–449, doi:10.1038/ngeo2155, 2014.

Shindell, D. T. and Schmidt, G. A.: Southern Hemisphere climate response to ozone changes and greenhouse gas increases, Geophy. Res. Lett., 31, L18209, doi:10.1029/2004GL020724, 2004.

Solomon, S.: Stratospheric ozone depletion: a review of concepts and history, Rev. Geophys., 37, 275–316, doi:10.1029/1999RG900008, 1999.

SPARC-CCMVal: SPARC CCMVal report on the evaluation of chemistry-climate models, SPARC Report No. 5, WCRP-132, WMO/TD-No. 152, 2010.

Taylor, K. E., Stouffer, R. J., and Meehl, G. A.: An overview of CMIP5 and the experiment design, B. Am. Meteorol. Soc., 93, 485–498, doi:10.1175/BAMS-D-11-00094.1, 2012.

Telford, P. J., Abraham, N. L., Archibald, A. T., Braesicke, P., Dalvi, M., Morgenstern, O., O'Connor, F. M., Richards, N. A. D., and Pyle, J. A.: Implementation of the Fast-JX Photolysis scheme (v6.4) into the UKCA component of the MetUM chemistry-climate model (v7.3), Geosci. Model Dev., 6, 161–177, doi:10.5194/gmd-6-161-2013, 2013.

Thompson, D. W. J., Solomon, S., Kushner, P. J., England, M. H., Grise, K. M., and Karoly, D. J.: Signatures of the Antarctic ozone hole in Southern Hemisphere surface climate change, Nat. Geosci., 4, 741–749, doi:10.1038/ngeo1296, 2011.

van der Werf, G. R., Randerson, J. T., Giglio, L., Collatz, G. J., Kasibhatla, P. S., and Arellano Jr., A. F.: Interannual variability in global biomass burning emissions from 1997 to 2004, Atmos. Chem. Phys., 6, 3423–3441, doi:10.5194/acp-6-3423-2006, 2006.

Webster, S., Brown, A. R., and Cameron, D. R.: Improvements to the representation of orography in the Met Office Unified Model, Q. J. Roy. Meteor. Soc., 129, 1989–2010, doi:10.1256/qj.02.133, 2003.

WMO (World Meteorological Organization): Scientific Assessment of Ozone Depletion: 2010, Global Ozone Research and Monitoring Project, Report No. 52, 516 pp., Geneva, Switzerland, 2011.

WMO (World Meteorological Organization): Scientific Assessment of Ozone Depletion: 2014, Global Ozone Research and Monitoring Project, Report No. 55, 416 pp., Geneva, Switzerland, 2014.

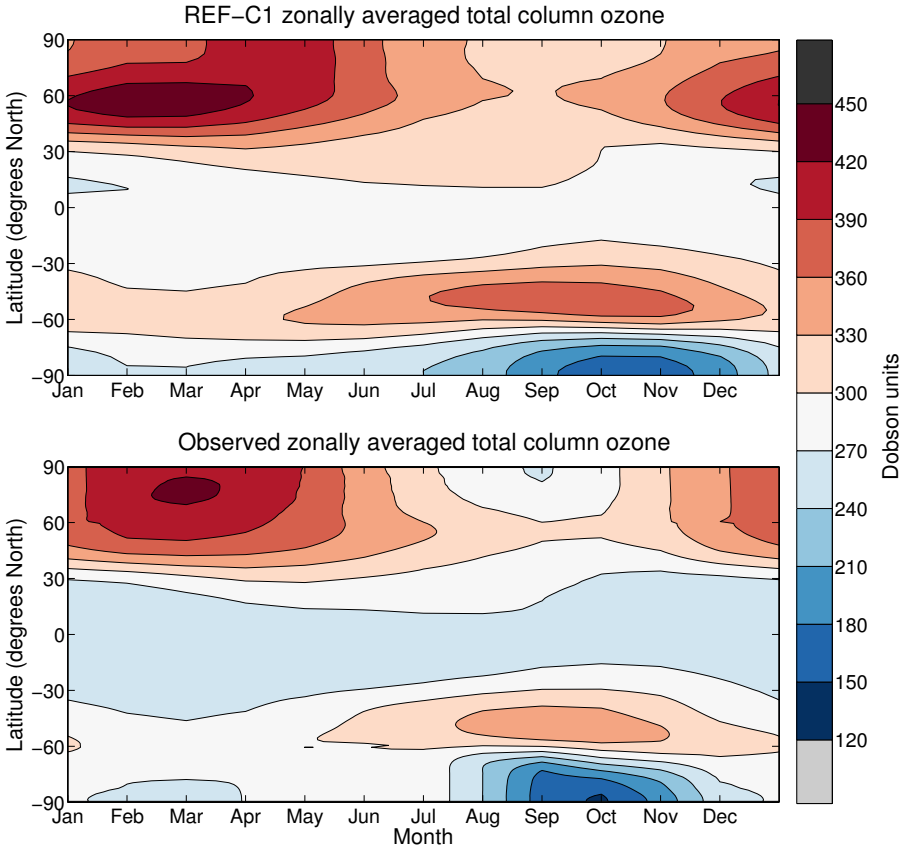

Figure 1. Zonally 2005–2010 averaged TCO for the REF-C1 hindcast simulation compared to observations from the Bodeker Scientific total column ozone database.

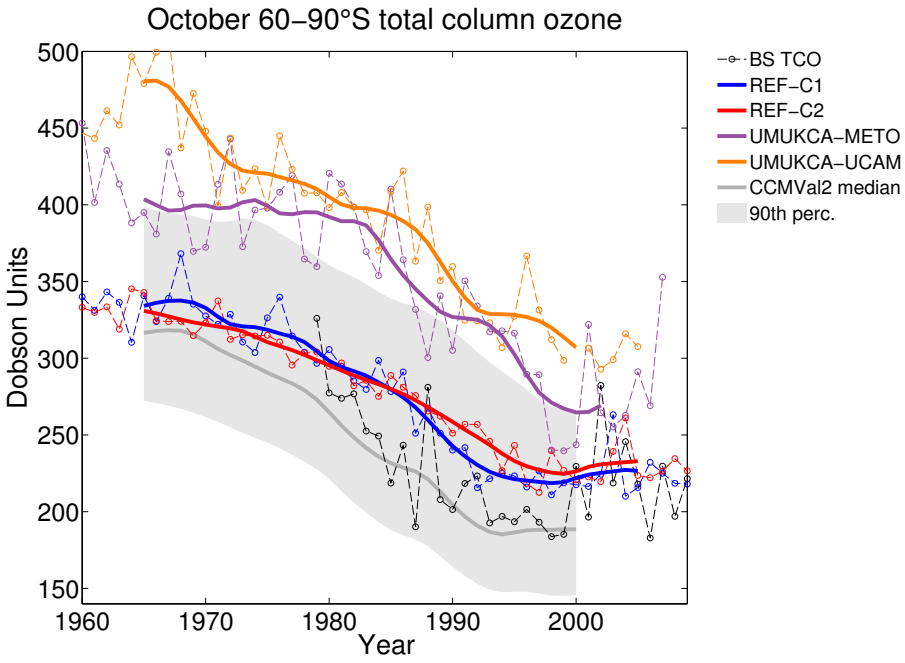

Figure 2. Time series of REF-C1 and REF-C2 TCO averaged between 60–90° S compared with the Bodeker Scientific total column ozone database observations, the UMUKCA-UCAM and UMUKCA-METO models and the CCMVal-2 ensemble. Dashed lines show the October average, while solid lines have undergone a 10 year running mean of October averages. The shaded region shows 10th and 90th percentiles of the CCMVal-2 ensemble.

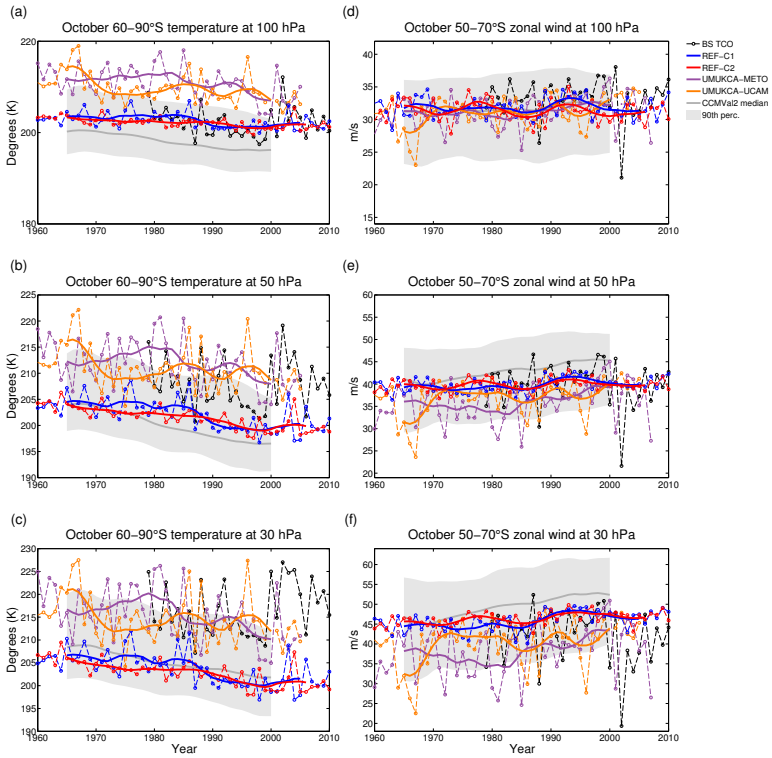

Figure 3. Time series of REF-C1 and REF-C2 temperature at **(a)** 100 hPa, **(b)** 50 hPa, and **(c)** 30 hPa averaged between 60–90° S and zonal wind at **(d)** 100 hPa, **(e)** 50 hPa, and **(f)** 30 hPa averaged between 50–70° S compared with ERA-Interim, the UMUKCA-UCAM and UMUKCA-METO models and the CCMVal-2 ensemble. The shaded region shows 10th and 90th percentiles of the CCMVal-2 ensemble.

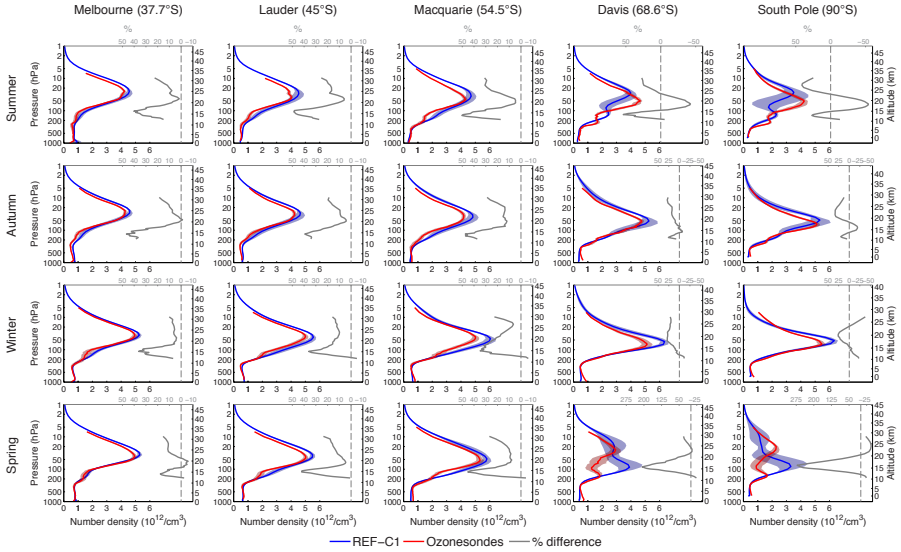

Figure 4. Seasonal average REF-C1 ozone profiles compared to ozonesondes for Melbourne, Lauder, Macquarie Island, Davis and the South Pole. REF-C1 and ozonesonde data are averaged between 2005–2010. Shaded regions show one standard deviation for REF-C1 and one standard deviation divided by $\sqrt{7.5}$ for the ozonesonde data. This is done for statistical consistency as monthly averaged output was used for the REF-C1 data (see Sect. 4.3 in the main text). Altitude values are approximate. The grey lines show REF-C1 percentage differences from ozonesondes, following the top x-axis.

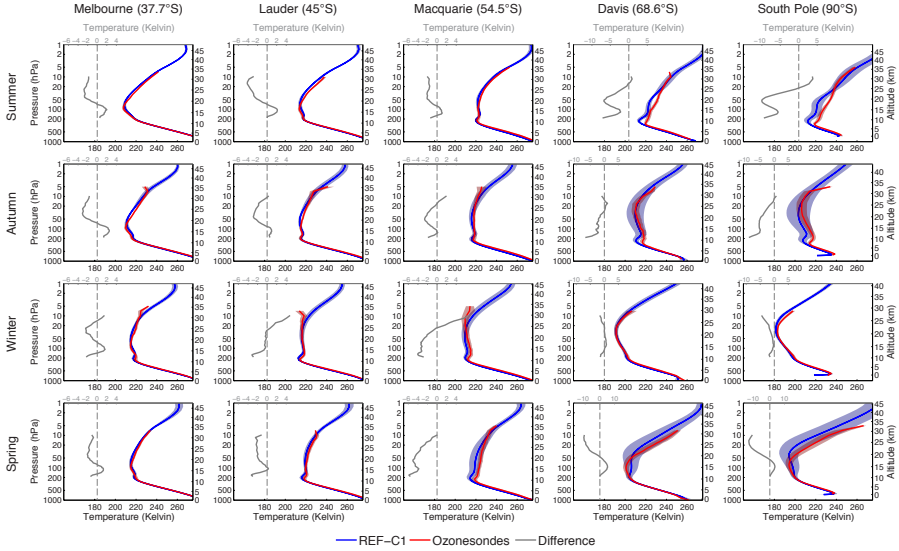

Figure 5. Same as Fig. 4, except for temperature. The grey lines show REF-C1 differences from ozonesondes, following the top x-axis.

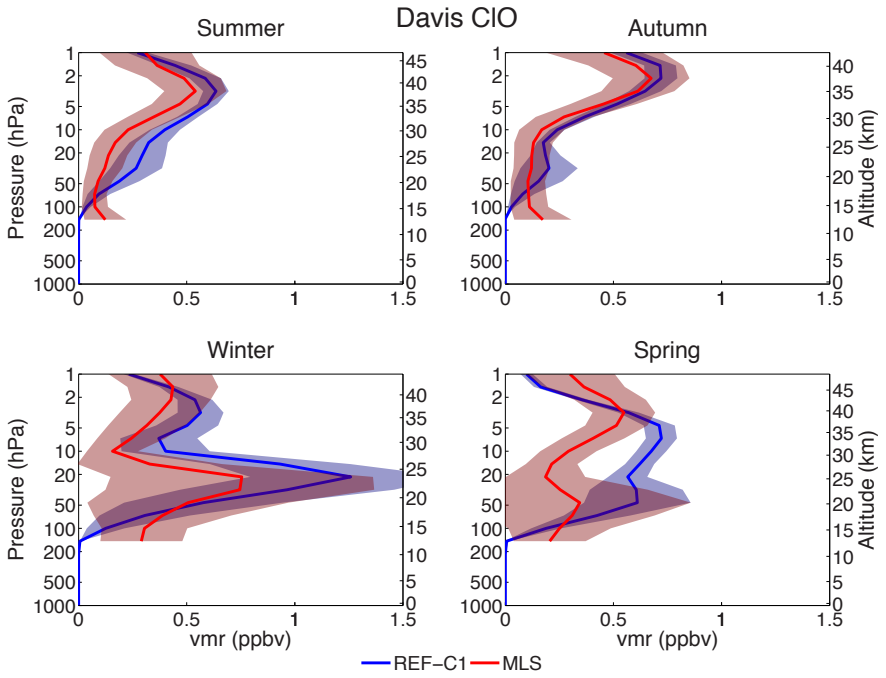

Figure 6. Comparison of seasonal average vertical profiles of ClO averaged between 67.5–70° S and 78.75–82.5° E. Seasonal average data is from 2005–2010 for REF-C1 and MLS. Shaded regions show one standard deviation. Altitude values are approximate.

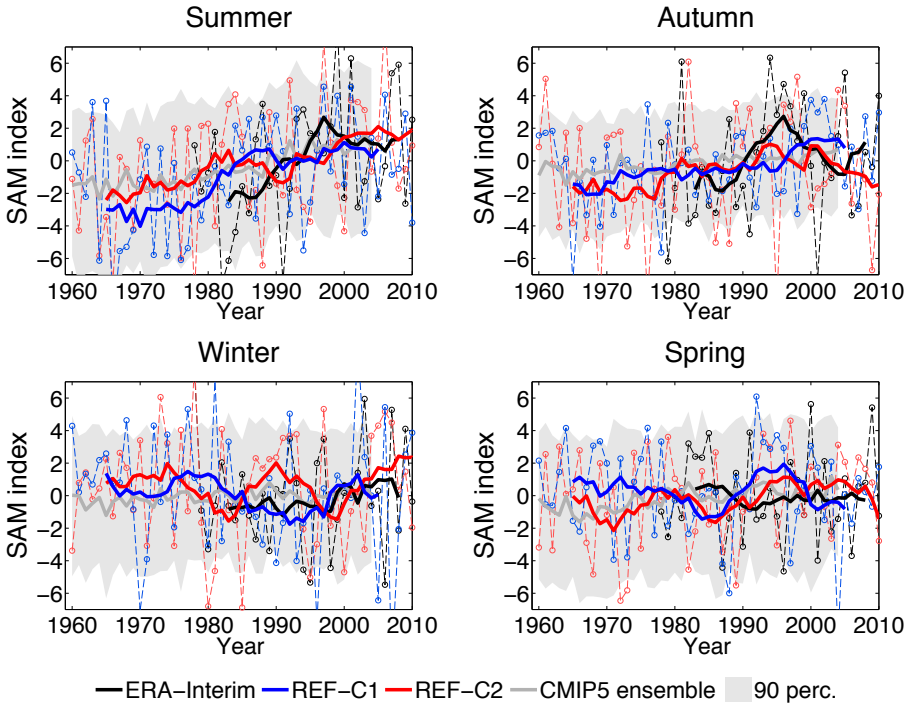

Figure 7. Seasonal SAM indexes for REF-C1 and REF-C2 simulations compared to ERA-Interim data and the CMIP5 ensemble. Dashed lines show seasonal averages, while the solid lines have undergone a 10 year running mean of seasonal averages. Shaded regions show the 10th and 90th percentiles of the CMIP5 ensemble.

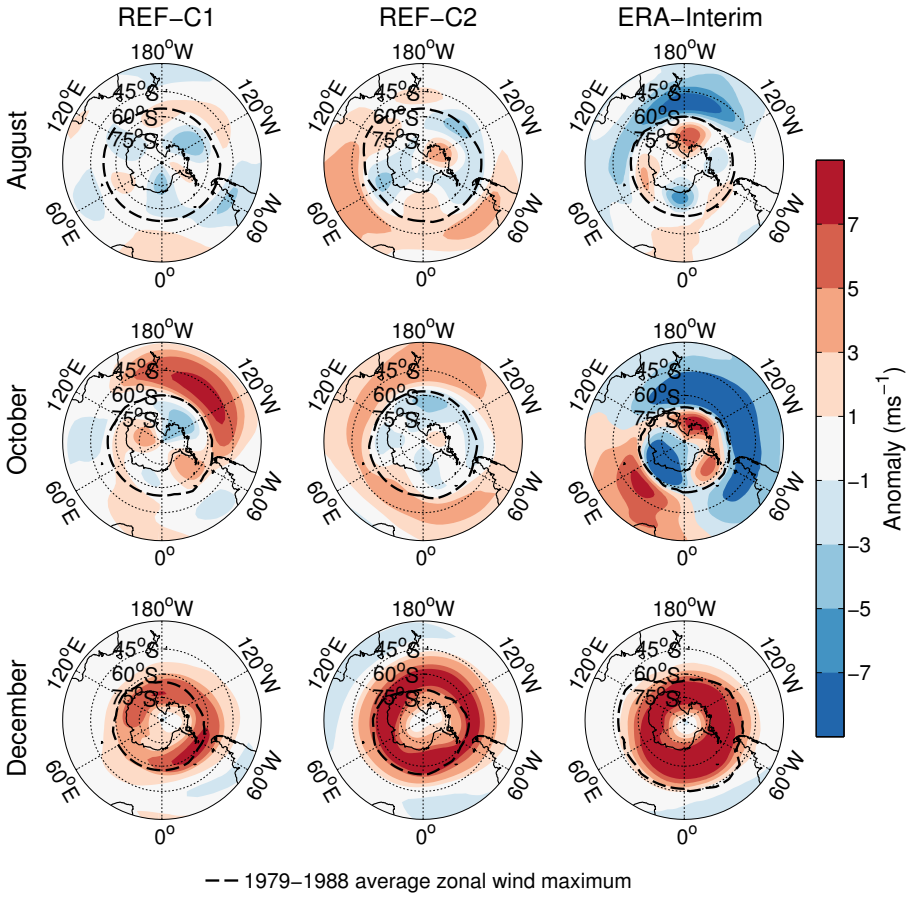

Figure 8. 2001–2010 minus 1979–1988 50 hPa zonal wind anomaly maps for REF-C1 and REF-C2 simulations compared to ERA-Interim data.